MEASUREMENTS AND ANALYSIS OF LONGITUDINAL HOM DRIVEN COUPLED BUNCH MODES IN PEP-II RINGS *

T. Mastorides†, C. Rivetta‡, J.D. Fox, D. Van Winkle
Stanford Linear Accelerator Center
Stanford, CA 94309, USA

Abstract

The growth rates of the longitudinal higher-order impedance-driven beam modes have greatly increased since the initial PEP-II design and commissioning. This increase is attributed to the addition of 6 1.2MW RF stations with 8 accelerating cavities in the HER and 2 1.2MW RF stations with 4 accelerating cavities in the LER, which allowed operations at twice the design current and almost four times the luminosity. As a result, the damping requirements for the longitudinal feedback have greatly increased since the design, and the feedback filters and control schemes have evolved during PEP-II operations.

In this paper, growth and damping rate data for the higher-order mode (HOM) driven coupled-bunch modes are presented from various PEP-II runs and are compared with historical estimates during commissioning. The effect of noise in the feedback processing channel is also studied. Both the stability and performance limits of the system are analyzed.

LONGITUDINAL INSTABILITIES

The PEP-II rings have exhibited coupled-bunch longitudinal instabilities since commissioning. The longitudinal instabilities in PEP-II are driven by two impedance sources: cavity fundamental and cavity HOM. The LLRF systems use direct and Comb loop feedback to reduce the effective impedance of the cavity fundamental. To further damp these instabilities two additional feedback systems are used: the Low Group Delay Woofer (LGDW) and the Longitudinal Feedback (LFB).

The band limited LGDW addresses the beam motion from in-cavity low-order modes via a signal from a beam pick-up and control paths through the RF stations [1], [2]. The cavity fundamental driven beam modes have been studied and predictions for higher currents, including studies of different configurations have been presented [3], [4].

The LFB is a wideband bunch by bunch channel that addresses all modes via a digital control filter and broadband longitudinal kickers. The LFB is needed to control instabilities from the cavity HOM impedance. It is a Digital Signal Processing (DSP) based flexible programmable system that can run FIR or IIR filters. A block diagram of the LFB system is shown in Figure 1.

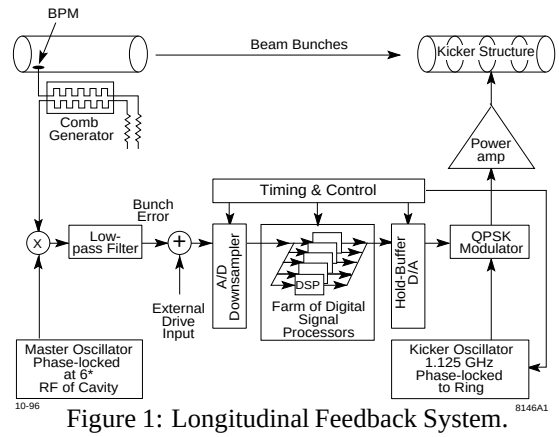

Figure 1: Longitudinal Feedback System.

This paper uses machine measurements in HER and LER to quantify the HOM driven growth rates, quantify the achieved performance of the broadband feedback, and highlight the performance limits in the systems as constructed [5].

HOM-DRIVEN MODES: GROWTH AND DAMPING RATES

During the PEP-II design and commissioning, the impedance driving beam instabilities was estimated from cavity measurements [6]. The impedance estimates allowed calculations of the expected growth rates for the HOM driven coupled-bunch modes, as shown in Figure 2 from [7]. The growth rates were calculated during commissioning for the design parameters of 1 A and 20 cavities for the HER and 2.25 A and 4 cavities for the LER. From this

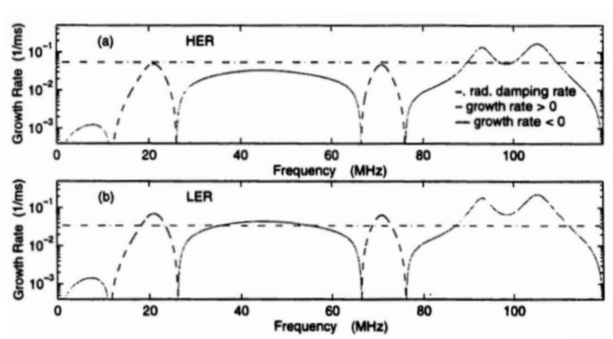

Figure 2: Growth Rate Estimates from Impedance Measurements for 1 A HER, 2.25 A LER.

figure one can see that there are two bands that excite instabilities. The strongest is a 9 MHz wide band that is aliased at around 105 MHz (mode 770) from the 238 MHz sampling and drives roughly 65 beam modes. The second band

* Work supported by the U.S. Department of Energy under contract # DE-AC02-76SF00515

† themis@slac.stanford.edu
‡ rivetta@slac.stanford.edu

is a 7 MHz wide band that aliases at around 93 MHz (mode 683). These wideband, instability driving impedances do not allow the use of narrowband feedback as employed for the cavity fundamental driven modes (LGDW). Furthermore, it is impossible to tune those impedances using adjustments in water temperature or cavity tuners. The dominant impedance driving these instabilities is the cavity HOM impedance, which is proportional to the number of cavities. The HOM driven coupled-bunch beam growth rates are proportional to the number of cavities and to the beam current.

At nominal current both rings exhibit coupled-bunch instabilities in the absence of the damping feedback systems. Therefore, to measure the beam growth rates, we open the LFB loop for a few milliseconds letting the unstable beam modes grow, and then turn it back on to recapture the beam [8], [9]. The time-domain data of the beam motion is transformed to a modal domain and fit versus time. The complex exponential fit provides an estimation of the modal growth rates and oscillation frequencies. This process allows the estimation of the fastest growing beam modes. Other techniques are possible to measure slower growing modes [10].

The highest HOM beam growth rates and the corresponding damping rates reported below are from a band between mode 790 and 810. This is very close to mode 770 that was estimated from the cavity data. The data reported are an average of the growth and damping rates over this mode range and multiple measurements.

HER For the HER, the HOM driven coupled-bunch modal growth rates are shown in Figure 3. Data points

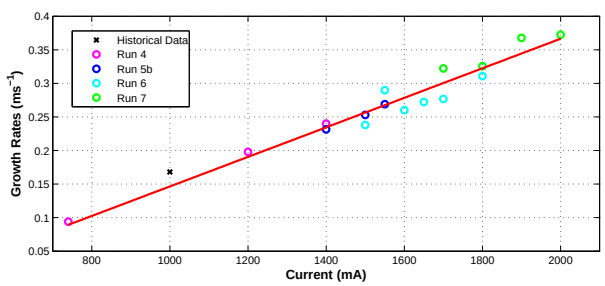

Figure 3: HER HOM driven coupled-bunch modal growth rates for modes 790-810.

over 4 years of PEP-II operations are collected. The data points show great linearity with current as expected. To correctly compare these data points, the data from run 4 have been multiplied by $14/13$ to account for the increase in the number of cavities from 26 to 28. The black point is a scaled version of the estimate based on the cavity data described above. The growth rate has been appropriately scaled by a factor of $28/20$ for the increase of the number of cavities from 20 to 28. Even though this point was estimated with limited resources more than ten years ago, it shows great agreement with our data.

The damping rates for the higher currents are shown in Figure 4. The LFB was configured with a 6 tap FIR filter centered around the 6 kHz synchrotron frequency. The kicker and digital processing gains are constant for all the

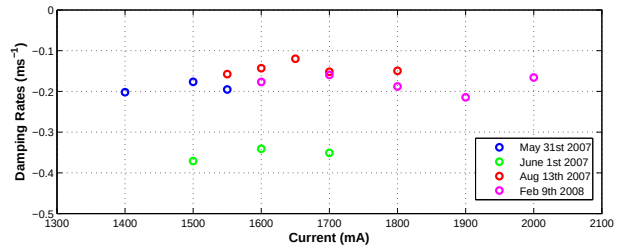

Figure 4: HER HOM driven coupled-bunch modal damping rates (growth plus feedback damping).

configurations shown. The filter gain is higher by a factor of 1.4 for the red and magenta data points. Even though the blue and green data points share the same configuration, they show a big difference in the modal damping rates. This difference is attributed to proper timing in the kicker. Changes in the order of tens of ps in the kicker timing exhibit huge improvement in the damping rates. Comparing the blue with the red and magenta data points, there is no improvement in the damping rate as expected with the higher filter gain due to the timing shifts. For the well-timed configurations, the damping margin was comparable to the measured growth rates, satisfying our margin criteria as defined in [4]. The lack of proportionality with current shows that the system is saturated. It should be noted though, that this saturation may be an artifact of the large longitudinal oscillations caused by the opening of the loop during our measurements. Even though we don't see this saturation during closed loop operation, it signifies that we are approaching limited headroom from saturation limits with this configuration.

LER For the LER, the HOM driven coupled-bunch modal growth rates are shown in Fig 5. The data is from

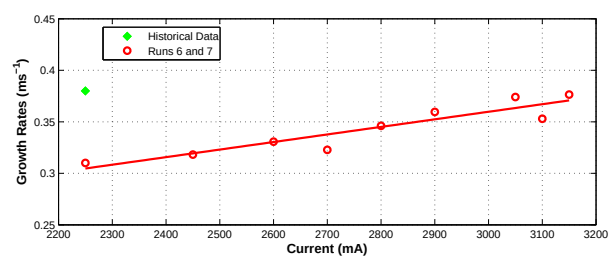

Figure 5: LER HOM driven coupled-bunch modal growth rates for modes 790-810.

runs 6 and 7 and shows great linearity with current as expected. Similarly to the HER, the green point is from the estimate based on the cavity data using the LER design parameters of 2 stations and 4 cavities. The growth rate has been appropriately scaled by a factor of 2 for the increase of the number of cavities from 4 to 8. Even though this point was estimated with limited resources more than ten years ago, it shows relative agreement with our data.

The corresponding modal damping rates are shown in Figure 6. The LFB was configured with a 10 tap FIR filter centered around the 4 kHz synchrotron frequency. The green and red data points share the same configuration. The filter gain of the blue data point is lower by a factor of 0.7,

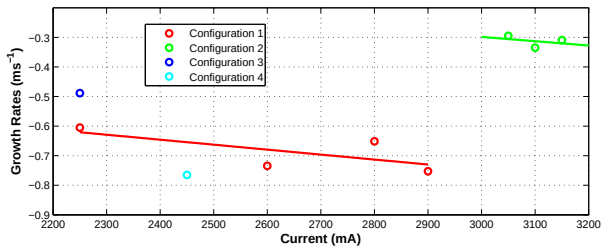

Figure 6: HER HOM driven coupled-bunch modal damping rates (growth plus feedback damping).

whereas the filter gain for the cyan data is higher by a factor of 1.4 from the green and red points. The red line is fitted to the red data points. As described in the HER case, the big difference between the red and green data points could be attributed to timing issues. Further analysis of our data will be conducted to determine whether there is a component of saturation reducing the performance at the higher currents. When the system is correctly timed, the damping margin was comparable to the measured growth rates, satisfying our margin criteria. The measurements agree with the expected behavior of increased damping rates with increasing gain and increasing current for the lower currents. The lack of direct proportionality though, signifies that we might be saturating our system.

Finally, Figure 7 shows the synchrotron frequencies for

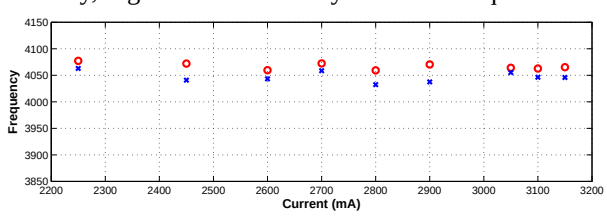

Figure 7: LER HOM driven coupled-bunch modal synchrotron frequencies.

the modal growth and damping rates with current. The two are in close agreement showing that the filter has been properly tuned for the system to introduce pure damping without affecting the modal oscillation frequency. The same check was performed in the HER with equally successful results.

FEEDBACK MODEL

To understand the effect of the system parameters in the LFB stability and performance, an analysis based on a dynamic model is presented. The model includes the dynamics of the multi-bunch beam, the loop filter, and the perturbing noise sources that degrade the performance and stability of the closed loop.

The multibunch system is a multiple-input, multiple-output (MIMO) system. It can be represented in a simplified version as depicted in Figure 8 [9], [11]. In absence of the LFB system damping the beam presents some unstable modes, defining an open loop unstable system. In addition, the system includes delays that in general limit the maximum open loop gain. The two main noise sources

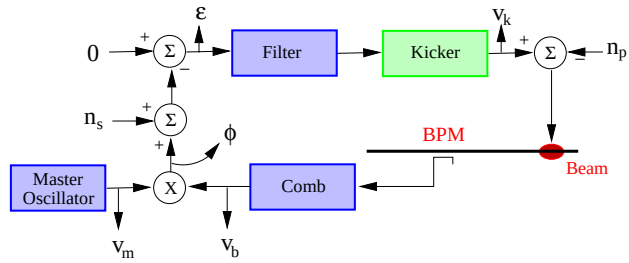

Figure 8: Simplified LFB Block Diagram.

in the system can be grouped in the process noise $n_p(t)$ and the sensor noise $n_s(t)$. The process noise collects mainly all the perturbations introduced by the RF stations, kicker timing, etc. The sensor noise describes mainly the collective effects of the noise in the receiver. This noise has sources in the Master Oscillator, kicker amplifiers, mixer, A/D sampler and cables connecting the BPM to the receiver. In a simple way, this noise can be analyzed assuming that the Master Oscillator produces a signal $v_m(t) = [V_m + n_m(t)]cos(\omega_0 t + \phi_m(t))$, where V_m is the amplitude of the sine wave, $\omega_0 = 6\,\omega_{RF}$, $n_m(t)$ and $\phi_m(t)$ are the amplitude and phase noise, respectively. The Comb filter responds to the beam impulses measured by the BPM with a finite duration signal $v_b(t, I_b) = [V_b(I_b) + n_b(t)]sin(\omega_0 t + \phi(t) + \phi_b(t))$, where $V_b(I_b)$ is the amplitude of the oscillation, proportional to the bunch intensity, $\phi(t)$ is the phase modulation in the beam produced by the noise $n_p(t)$ and the kicker signal, $n_b(t)$ and $\phi_b(t)$ are the amplitude and phase noise respectively, induced in the burst $v_b(t)$ by Johnson noise and pick-up.

The action of the mixer can be then simplified as $v_b(t, I_b)\, v_m(t) + n_x(t)$, where $n_x(t)$ is noise of the mixer at the output. Eliminating the upper sidebands at the mixer output by filtering, the detected signal is approximately $0.5\ [V_b(I_b)V_m sin(\phi)] + n_A sin(\phi) + n_\phi + n_x$, where $n_A = 0.5\ [V_m n_b + V_b(I_b)n_m]$ and $n_\phi = 0.5\ V_b(I_b)V_m cos(\phi)[\phi_b + \phi_m]$. To complete the model of the sensor noise $n_s(t)$, the ADC noise can be included giving $n_s(t) = n_A sin(\phi) + n_\phi + n_{ADC} + n_x$. It is important to notice that since the Comb generator output signal is proportional to the bunch intensity (beam current), the gain of the phase detector is proportional to the beam current and the noise of the receiver $n_s(t)$ increases also with the beam intensity.

The beam dynamics of each bunch are modeled as a discrete harmonic oscillator driven periodically ($6T_{rev} = 44.1\mu sec.$) by 6 equally spaced impulses with equal amplitude. This represents the effect of kicking individually each bunch at the revolution frequency by a system that has a downsampling factor of 6. Additionally, the destabilizing effect of the cavity HOM impedance is included in this model.

The set of transfer functions representing the ratio between the individual kicker signals $V_k(t)$ and the corresponding error signal $\epsilon(t)$ is defined mainly by the loop filter transfer function (FIR or IIR filters). This processing acts individually on the error signal generated by each

bunch and generates a control signal $V_k(t)$ that kicks the same bunch a few turns later.

Mathematically, the system depicted in Fig. 8 can be transformed into a modal domain using the transformation T, where the (m, l) element is defined by $T(m, l) = e^{-j2\pi \frac{ml}{N}}$. One advantage of the representation of the system in the modal frame is that the parameters defining the beam dynamic model for the unstable modes can be easily estimated form the growth rate measurements presented in the previous Section. Additionally, for the bank filter structure used in the LFB, where each filter processes the signal of an individual bunch, the transfer function of the filter is invariant with respect to the transformation.

The filter bank in the LFB is designed to stabilize the multibunch beam dynamics. There is a set of equal filters which stabilize the most unstable beam mode, and consequently all other beam modes. The design of the LER LFB loop filter follows. At $I_b = 2250mA$, from Figs. 5 and 7, the eigenvalues of the dominant unstable mode are $\Lambda = (+0.3 \ \pm j \ 2\pi \ 4.070) \ ms^{-1}$. The transfer function of the beam for that particular mode is shown in Fig. 9. For

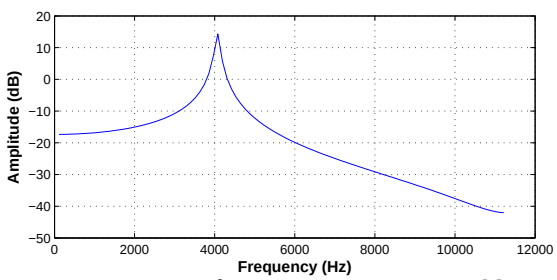

Figure 9: Beam Transfer Function - Most unstable mode.

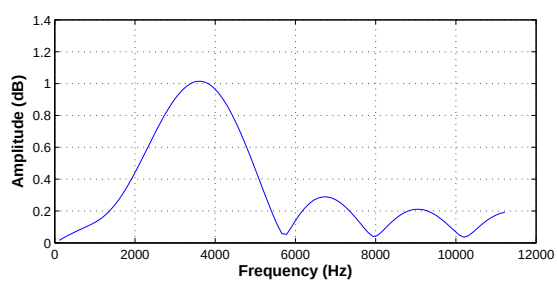

Figure 10: 10-Tap Loop Filter magnitude Transfer Function.

this system, a 10-tap FIR filter was designed. Its magnitude transfer function is depicted in Fig. 10.

When operating in closed loop, the eigenvalues of the composite system can be analyzed in the complex plane based on the Z-domain root locus analysis. Fig. 11 depicts the root locus for this particular system for open loop gains ranging from 0 to 3. Black squares show the location of the open loop eigenvalues of the composite system, as defined by the modal beam unstable eigenvalues and multiple eigenvalues defined by both the system and filter delays. The circles represent the zeros of the system defined mainly by the zeros of the filter. It is possible to evaluate the location of the closed loop eigenvalues for different gains for this particular beam mode. From the zoomed part in Figure 11 it is possible to observe that there is a min-

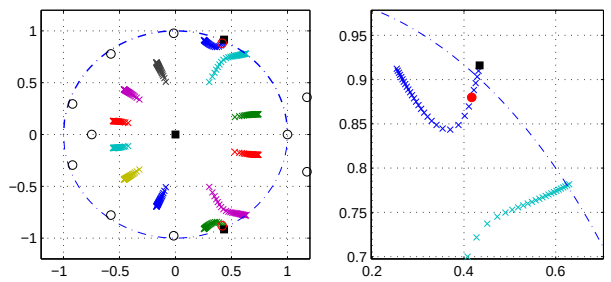

Figure 11: Root Locus.

imum gain to stabilize that particular beam mode, setting the closed-loop eigenvalues over the unity circle (open loop gain = 0.2). Additional gain is necessary to set the closed-loop eigenvalues to the red circle in the zoomed locus at $\Lambda = (-0.6 \ \pm j \ 2\pi \ 4.070) \ ms^{-1}$ (gain 0.5). This condition corresponds to Fig.8. For open loop gain greater than 3 one observes that the system is unstable.

NOISE FLOOR MEASUREMENTS

In order to quantify the effect of the noise sources in the LFB system in both PEP-II rings, several noise measurement were performed using the built-in data acquisition system of the LFB. The downsampled signal digitized at 238 Msamples/sec by the ADC is recorded for offline analysis. This corresponds to the error signal $\epsilon(t)$ depicted in Fig. 8. The acquired signal is post-processed to calculate the noise spectrum. We estimate the power spectrum bunch by bunch and a quadrature average provides the equivalent noise spectrum of mode 0 in the modal domain.

To analyze the impact of the different noise sources, measurements were conducted in several configurations. Terminating the ADC input with 50 Ohms provides a measure of $n_{ADC}(t)$ – the quantizing noise in the A/D and the noise in the internal sampler (as well as any systematic clock noise present in the processing). Turning off the gain in the Comb path at 3 GHz measures the noise contribution from the baseband channel plus the noise contribution through the mixer and Master Oscillator. Finally, measuring the system in the nominal channel configuration but in the absence of beam quantifies the sensor noise $n_s(t)$ – the noise contribution from the whole RF path and processing channel (including any coherent pickup in cables, BPM, etc). It is important to notice that the noise source $n_s(t)$ defined in our model includes noise terms that are amplified by the amplitude of the Comb generator signal $V_b(I_b)$. The other two measurement mentioned above cannot quantify completely these noise terms since $V_b(I_b) \simeq 0$ in these cases.

Measuring the noise of the system with beam quantifies the impact of both noise sources $n_s(t)$ and $n_p(t)$ in Figure 8. In closed loop the effect of these sources in the ADC is now affected by the transfer functions of the LFB system. These transfer functions will filter differently the perturbations due to the receiver noise $n_s(t)$ and the process noise $n_p(t)$.

LER noise measurements Figure 12 shows the noise levels for the four cases described above. Label 'A/D'

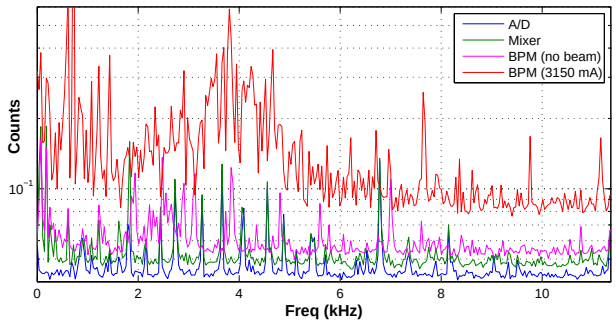

Figure 12: LER noise measurements.

identify the measurement of n_{ADC}, 'mixer' represents the case with the Comb gain turned off, 'BPM (no beam)' shows n_s, and 'BPM (3150 mA)' indicates the closed loop case with beam present. The measurements exhibit the expected order of noise power magnitude. For the LER, the noise in rms equivalent counts at the output of the ADC is approximately 0.66. To show the non-ideality and additional effects in the implemented A/D converter, a perfect quantizer, would have 0.32 rms counts of quantization noise. It is important to observe that the beam noise is dominant and much greater than the other measurements. Part of the noise is amplified by the system around the synchrotron frequency at 4.07 kHz. The noise spectrum with beam shows large noise interference at 720 Hz and 1440 Hz, which correspond to the RF klystron High Voltage power supply ripple. Again, since in the presence of beam we have almost 2 rms counts of noise, increasing the number of bits in the A/D would have no effect on the system noise. A 6 bit A/D would still have a noise level comparable to the beam noise. To improve the system closed loop rms noise floor we either have to improve our kicker amplifiers or to reduce the RF station noise (that drives the beam noise spectrum at low frequencies) through a narrower LFB filter or through other station improvements.

HER noise measurements Figure 13 shows measurements for the HER, exhibiting the same characteristics as the LER. We again see how the RF station noise amplified

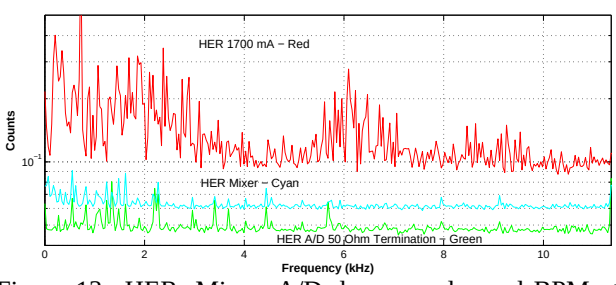

Figure 13: HER: Mixer, A/D downsampler and BPM at 1700mA.

through the beam dominates our system. In the HER case the synchrotron frequency is close to 6 kHz as can be inferred from the spectrum.

CONCLUSIONS

The LFB system was designed for much lower currents. Its programmable design allowed operations with much larger growth rates. Even though the system still had sufficient gain margin, the noise coupled to the beam from the RF station was very close to saturating the LFB at the highest beam currents. To operate at even higher currents, additional kicker power or improvements in the LLRF would have been necessary. Another important limitation was the kickers timing. We see that timing shifts in the ps level reduced the system gain – and thus the stability and margin – substantially.

ACKNOWLEDGEMENTS

The authors would like to thank D. Teytelman, S. Prabhakar, and H. Hindi for all their work, help and ideas that provided a substantial base to build on. We would also like to thank the PEP-II operations and accelerator groups for their consistent help with these measurements, the SLAC ART department and SSRL accelerator physics department for many helpful collegial discussions. We acknowledge our colleagues at LBL, LFN and KEK who have shared their ideas and interests on this subject.

REFERENCES

[1] D. Teytelman *et. al.*, "Operating Performance of the Low Group Delay Woofer Channel in PEP-II", PAC 2005.

[2] D. Teytelman *et. al.*, "Development and Testing of a Low Group-Delay Woofer Channel for PEP-II", EPAC 2004.

[3] T. Mastorides *et. al.*, "Analysis of Longitudinal Beam Dynamics Behavior and RF System Operative Limits at High Beam Currents in Storage Rings", submitted to Phys. Rev. ST-AB.

[4] C. Rivetta *et. al.*, "Modeling and Simulation of Longitudinal Dynamics for Low Energy Ring-High Energy Ring at the Positron-Electron Project", Phys. Rev. ST-AB, 10, 022801 (2007).

[5] D. Teytelman *et. al.*, "Control of Multibunch Longitudinal Instabilities and Beam Diagnostics Using a DSP-Based Feedback System", PAC 1997.

[6] R. Rimmer *et. al.*, "Updated Impedance Estimate of the PEP-II RF Cavity", EPAC 1996.

[7] S.Prabhakar, "New Diagnostics and Cures for Coupled Bunch Instabilities", Thesis, Stanford University Applied Physics Dpt., August 2001.

[8] S.Prabhakar *et. al.*, "Observation and Modal Analysis of Coupled-Bunch Longitudinal Instabilities via a Digital Feedback Control System", Part.Accel.57:175-187, 1997.

[9] D.Teytelman, "Architectures and Algorithms for Control and Diagnostics of Coupled-Bunch Instabilities in Circular Accelerators", Thesis, Stanford University EE Dpt., June 2003.

[10] J. Fox *et. al*, "Multi-bunch Instability Diagnostics via Digital Feedback Systems at PEP-II, DAΦNE, ALS and SPEAR", PAC 1999.

[11] H. Hindi *et. al.*, "Analysis of DSP-Based Longitudinal Feedback System: Trials at SPEAR and ALS", PAC 1993.